HHS Public Access

Author manuscript

ACS Chem Biol. Author manuscript; available in PMC 2019 August 17.

Published in final edited form as:

ACS Chem Biol. 2018 August 17; 13(8): 2121–2129. doi:10.1021/acschembio.8b00290.

The Biochemical Basis of Vitamin A Production from the Asymmetric Carotenoid β-Cryptoxanthin

Mary E. Kelly[1], **Srinivasagan Ramkumar**[1], **Weizhong Sun**[1], **Crystal Colon Ortiz**[1], **Philip D. Kiser**[1], **Marcin Golczak**[1], and **Johannes von Lintig**[1,*]

[1]Department of Pharmacology, Case Western Reserve University School of Medicine, Cleveland, OH 44106

Abstract

Vitamin A serves essential functions in mammalian biology as a signaling molecule and chromophore. This lipid can be synthesized from more than 50 putative dietary provitamin A precursor molecules which contain at least one unsubstituted β-ionone ring. We here scrutinized the enzymatic properties and substrate specificities of the two structurally related carotenoid cleavage dioxygenases (CCDs) which catalyze this synthesis. Recombinant BCO1 split substrates across the C15,C15' double bond adjacent to a canonical β-ionone ring site to vitamin A aldehyde. Substitution of the ring with a hydroxyl group prevented this conversion. The removal of methyl groups from the polyene carbon backbone of the substrate did not impede enzyme activity. Homology modeling and site directed mutagenesis identified amino acid residues at the entrance of the substrate tunnel which determined BCO1's specificity for the canonical β-ionone ring site. In contrast, BCO2 split substrates across the C9,C10 double bond adjacent to assorted ionone ring sites. Kinetic analysis revealed a higher catalytic efficiency of BCO2 with substrates bearing 3-hydroxy-ionone rings. In the mouse intestine, the asymmetric carotenoid β-cryptoxanthin with one canonical and one 3-hydroxy-β-ionone ring site was meticulously converted to vitamin A. The tailoring of this asymmetric substrate occurred by a stepwise processing of the carotenoid substrate by both CCDs and involved a β-apo-10'-carotenal intermediate. Thus, opposite selectivity for ionone ring sites of the two mammalian CCDs complement each other in the metabolic challenge of vitamin A production from a chemically diverse set of precursor molecules.

Graphical Abstract

*To whom correspondence should be addressed: Johannes von Lintig, Department of Pharmacology, Case Western Reserve University, School of Medicine, 2109 Adelbert Rd. W341, Cleveland, OH 44106, Tel.: (216)-368-3528, Fax: (216) 368-1300; johannes.vonlintig@case.edu.

AUTHOR CONTRIBUTIONS

M.K. and J.v.L. designed and performed research, analyzed data and wrote the manuscript. R.S., W.S., C.C.O., P.K., and M.G. performed research and analyzed data.

CONFLICT OF INTEREST

The authors declare no competing financial interest.

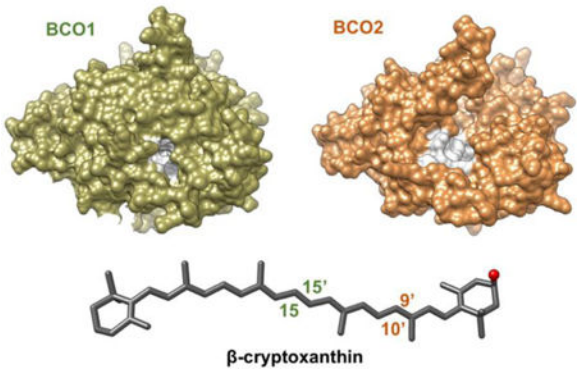

Keywords

β-cryptoxanthin; BCO1; BCO2; Carotenoid Cleaving Dioxygenase

Carotenoids are a class of isoprenoid pigments synthesized by plants, fungi, and bacteria by the condensation of eight isoprenoid units. The enormous chemical diversity of carotenids (more than 600 compounds) results from modulation of their polyene chromophores, shifting of their conjugated double bonds, and the addition of functional groups to their terminal ionone rings (1). Carotenoids can be chemically transformed to a myriad of apocarotenoid metabolites (2). These molecules play important roles as chromophores and signaling molecules in all kingdoms of living nature (3). Mammals acquire carotenoids from the diet and metabolize them to vitamin A aldehyde, from which all biologically active retinoids can be synthesized, including the visual chromophore and retinoic acid. Retinoic acid regulates gene expression throughout the mammalian life cycle and is responsible for most extra-visual effects of vitamin A (4).

Enzymatic oxidative cleavage of carotenoids at a specific position of the polyene chain has been proposed as the method for apocarotenoid production. This conversion is mediated by an ancestral family of carotenoid cleavage dioxygenases (CCDs) (5). CCDs are non-heme iron oxygenases with a characteristic tertiary structure comprised of a rigid seven-bladed β-propeller covered by a half-dome (6). The ferrous iron in the active center is accessible through a long, non-polar tunnel lined with hydrophobic residues that likely act as conduits for passage of the lipophilic substrates (7, 8). The role of ferrous iron in double bond cleaving CCDs is to activate diatomic oxygen for cleavage of carotenoids (9–11). The subsequent reaction follows a dioxygenase mechanism in which both oxygen atoms are incorporated into the apocarotenoid products (12–14).

The mammalian genome encodes three different types of CCDs (15). The β-carotene-15,15′-dioxygenase (BCO1) and the β-carotene-9’,10’-dioxygenase (BCO2) enzymes catalyze the oxidative cleavage across double bonds at the C15,C15’ and C9’,C10’ positions on the carbon backbone of carotenoids, respectively (16). A third family member, the retinal pigment epithelium-specific 65 kDa protein (RPE65) does not retain the double bond cleavage activity of BCO1 and BCO2 and catalyzes a combined ester cleavage and

double bond isomerization at position C10,C11 reaction of retinyl esters (RE) into 11-*cis*-retinal (17).

Food contains a diverse set of carotenoids, from which about 50 exert provitamin A activity (18). These provitamin A carotenoids must contain at least one unsubstituted β-ionone ring to be converted to retinoids. These compounds include the symmetric β,β-carotene (BC) as well as asymmetric β,ε-carotene (α-carotene, AC) (19) and 3R-β,β-Caroten-3-ol (β-cryptoxanthin, CX) (20). In the test tube, recombinant BCO1 splits asymmetric provitamin A precursors into canonical and non-canonical retinaldehyde moieties (21, 22). Recombinant BCO2 also converts these compounds into various apocarotenoids (23–26). Hence the enzymatic conversion of a single provitamin A could result in many distinct cleavage products which could be further metabolized to a large number of alcohols, acids, and geometric isomers. Surprisingly, only retinoids (vitamin A and its metabolites) accumulate in significant amounts in mammalian plasma and tissues. However, mechanisms that promote the production of retinoids over other apocarotenoids from dietary carotenoid precursors have yet not been delineated.

RESULTS AND DISCUSSION

A great multitude of dietary carotenoids exists but mammals express only two CCD enzymes to metabolize them. Recombinant BCO1 and BCO2 display a high degree of substrate promiscuity (16, 21–23, 25, 27, 28). This substrate promiscuity is not only an interesting question with regards to enzymology but provides a challenge for vitamin A biology. Production of certain apocarotenoids and non-canonical retinoids by these enzymes would pose a threat to vitamin A biology (24, 29–31). However, these products are largely absent in the *in vivo* setting. This poses the question how mammals can accurately, efficiently, and effectively metabolize many provitamin A substrates to produce vitamin A. In this work, we describe how nature's engineering exploit has generated an enzyme system which can cope with this metabolic challenge.

Probing enzymatic properties of CCDs with model substrates

We expressed and purified recombinant human BCO1 and mouse BCO2 containing an N-terminal His-tag in *E. coli* cells (Fig. 1a, b). The identities of BCO1 and BCO2 were confirmed by Western blot analysis (Fig. 1a, b). To identify functional groups of the carotenoid substrates that interact with either BCO1 or BCO2, we employed natural and synthetic carotenoids (Fig. 1c, d and Fig. S1 and Fig. S2). As expected, BCO1 catalyzed the production of all-*trans*-retinal from BC (Fig. S1a). From AC and CX, production of all-*trans*-retinal and the respective ε-retinal and 3-hydoxy-retinal were catalyzed by the enzyme (Fig. 1a and Fig. S1B). The all-*trans*-ε-retinal-oxime and all-*trans*-retinal-oxime products resulting from AC cleavage were not separated by our HPLC system (Fig. S1b). In contrast, all-*trans*-retinal and all-*trans*-3-hydroxy-retinal resulting from CX cleavage displayed distinct retention times and existed in approximately equimolar ratio (Fig. 1a). We also assessed the contribution of the methyl groups in the carbon backbone of the substrate using 20,20'-di-nor-BC. HPLC analyses revealed the production of 20-nor-retinal, indicating that the dual lack of methyl groups at C20 and C20' did not affect BCO1's activity (Fig. S1c).

When 15,15'-dehydro-BC was incubated with BCO1 no product formation was observed, indicating that the replacement of the scissile double bond by a triple bond rendered BCO1 inactive (Fig. S1d).

Incubations with recombinant mouse BCO2 yielded β-apo-10'-carotenal (APO10al) formation from BC and AC (Fig. S2a,b). BCO2 produced 2.5 fold more product when incubated with AC than with BC when equal amounts of enzyme and substrate were used (Fig. S2a,b). We also observed apocarotenoid formation when we removed methyl groups from the carbon backbone of BC (Fig. S2c). Notably, the production of APO10al was highly increased when BCO2 was incubated with CX (Fig. 1b). Some 3-hydroxy-APO10al was also present in these extracts (Fig. 1b). The production of higher amounts of APO10al versus 3-hydroxy-APO10al (8 to 1) showed that BCO2 preferentially cleaved across the C9,C10 double bond adjacent to the hydroxylated β-ionone ring site of CX. This preference was further confirmed by incubations with 3,3'-di-hydroxy-BC (zeaxanthin, ZEA) from which BCO2 removed both hydroxylated β-ionone rings to produce the dialdehyde rosafluene (Fig. S2d).

Elucidating the pathway for vitamin A production in mouse intestine

We previously discovered clues leading to the dissection of the carotenoid metabolic pathway using knockout mouse models. These studies clearly showed that BCO1 is required for BC metabolism (24, 32), and that BCO2 is required for the metabolism of non-provitamin A carotenoids, including ZEA, lutein, and lycopene (33, 34). To probe *in vivo* the contributions of the two CCDs to the metabolism of an asymmetric provitamin A carotenoid, we employed mice lacking the transcription factor ISX ($Isx^{-/-}$mice). These mice display significantly higher intestinal carotenoid absorption and conversion rates than wild type (WT) mice (35). As model carotenoids, we used the symmetric BC and the asymmetric CX. We fasted mice overnight and gavaged them with a pharmacological dose of carotenoids. Two hours after gavage, mice were sacrificed and the jejunums were dissected. By q-RT-PCR analysis, we confirmed that BCO1 and BCO2 were highly expressed in intestine of $Isx^{-/-}$mice, with Ct values of 29.51±0.32 and 26.98±0.02, respectively. We next extracted lipids from the thoroughly rinsed jejunum and subjected the extracts to a three step gradient HPLC analysis. We used synthetic standards for retinoids and APO10al and APO10ol and prepared 3-hydroxy-retinoids by incubating ZEA with the insect enzyme NinaB (12). In the first gradient step, BC andRE eluted; in the second gradient step, APO10al/ol, and all-*trans*-retinol (ROL) eluted; in the third gradient step, 3-hydroxy-retinoids eluted (Fig. 2a). In intestinal extracts of BC gavaged mice, parent BC, retinyl esters and ROL were detected as major metabolites (Fig. 2a and Table S1). In CX gavaged mice (Fig. 2a,c and Table S1), we identified RE in the fraction eluted in step 1. In the fraction eluted in step 2, 3-oxo-CX, parent CX, and ROL were detected (Fig. 2a,c and Table S1). Additionally, we observed significant amounts of APO10al and APO10ol in this fraction (Fig. 2b,c and Table S1). The latter substances were identified by their spectral characteristics and retention time as compared to authentic standard substances (Fig. 2b,c and Table S1). Notably, in the fraction eluted in step 3, we did not detect any 3-hydroxy-retinoids in the CX gavaged cohort (Fig. 2a,c and Table S1). The absence of 3-hydroxy-retinoids was further confirmed upon saponification of the intestinal extracts (data not

shown). Thus, we observed that CX, like BC, was exclusively converted to canonical vitamin A.

Analysis in CCD knockout mice

The absence of 3-hydroxy-retinoids and the presence of APO10al in the intestine of CX gavaged *Isx*$^{-/-}$mice indicated that the conversion of CX to vitamin A involved stepwise processing by both CCD enzymes (Fig. 2). To further probe this assumption, we analyzed the consequences of deficiency of either CCD on the metabolism of CX. Thus, we subjected WT, *Bco1*$^{-/-}$, and *Bco2*$^{-/-}$mice to vitamin A deprivation for 2 weeks and gavaged them thereafter with three consecutive doses of CX (Fig. 3a). After the last gavage, animals were sacrificed, blood was collected and livers were dissected. HPLC analysis showed that both CCD-deficient mouse lines but not their WT counterparts accumulated CX in serum and liver (Fig. 3b,d). In the serum of these mice, CX existed as parent (3-hydroxy) and as oxidized (3-oxo) forms (Fig. 3b). We next analyzed whether apocarotenoids are formed in the absence of either CCD. In saponified hepatic lipid extracts, APO10ol was detectable in *Bco1*$^{-/-}$mice but was absent in *Bco2*$^{-/-}$and WT mice (Fig. 3d and Fig. S3). Together, these analyses provided evidence that CX metabolism depends on functional BCO1 and BCO2 alleles. In both CCD-deficiencies, CX accumulated in serum and liver. In BCO2-deficient animals, CX was oxidized to its corresponding 3-oxo-derivative. In BCO1 deficient mice, CX was metabolized at least in part to APO10ol. In WT mice, however, CX was efficiently and completely metabolized.

β-apocarotenoid assays exposed ionone-ring site selectivity of CCDs

Our analyses in mice provided evidence that sequential cleavage by both CCDs constitutes a method for the conversion of CX to canonical retinoids. Critical for this proposed pathway would be selectivity of the two mammalian CCDs for specific ionone ring sites. Previously, it has been reported that the catalytic efficiency of human BCO1 for BC with two canonical β-ionone ring sites is far higher than for CX (21, 22). Contrarily, BC is a poor substrate for BCO2 (25) and the conversion of CX with two different ionone ring sites follows complex kinetics (Fig. S4). Therefore, we took advantage of mono-cyclic β-apo-8'-carotenal (APO8al) and 3-hydroxy-APO8al substrates. With BCO1 (Fig. 4a-c), HPLC analysis of extracted lipids showed that all-*trans*-retinal was produced from APO8al (Fig. 4b). In contrast, no 3-hydroxy-retinal (retention time 14.5 min) was detectable in repeated assays when BCO1 was incubated in the presence of 3-hydroxy-APO8al (Fig. 4c), indicating that hydroxylation of the β-ionone ring prevented enzymatic conversion of the substrate.

We next tested whether BCO2 can distinguish between different ionone rings sites. When incubated with APO8al, a product which eluted at 7.5 min from the column was produced (Fig. 4d). We obtained the same compound when BCO2 was incubated with 3-hydroxy-APO8al (Fig. 4e). This finding indicated that BCO2 removed the ionone ring sites in each substrate by oxidative cleavage across the C9,C10 double bond to produce the respective β-ionone and 10,8'-diapocarotene-10,8'-dial. The identity of 10,8'-diapocarotene-10,8'-dial resulting from this reaction was verified by mass spectrometry (Fig. 4f).

We next performed kinetic analysis with BCO2 and the two different apocarotenoids (Fig. 5). For this purpose we established a test protocol in which the enzyme was incubated in the presence of 0.1% Triton X-100, which allowed us to test a wide range of substrate concentrations (2 to 40 μM). To determine V_{max} and k_{cat} for different substrates, the same purified BCO2 enzyme preparation was used and extraction efficiencies were normalized by an internal standard. Mathematical analyses of the obtained data sets demonstrated that BCO2 displayed Michaelis Menten kinetics with both substrates (Fig. 5). The K_M values for the two substrates were within the low μM range. However, BCO2 displayed significant higher V_{max} and k_{cat} values with 3-hydroxy-APO8al than APO8al (Fig. 5). The ratio k_{cat}/K_M, often referred to as the 'specificity constant', is a useful index for comparing the relative rates of an enzyme acting on alternative, competing substrates. This constant was an order of magnitude higher for 3-hydroxy-APO8al than for APO8al (Fig. 5).

The structural basis of ionone ring site selectivity of mammalian CCDs

Mammalian CCDs share about 40% sequence identity and a conserved basic structural fold. We choose the crystal structure of RPE65 bound to emixustat and palmitate as the template for homology modeling software to predict how BCO1 and BCO2 might interact with their substrates (36). Emixustat, co-crystallized with RPE65, is a competitive inhibitor (IC_{50}=232 nM) (Fig. S5) (36). To test whether emixustat inhibited BCO1 as well, we performed enzyme assays and observed no significant inhibition of enzymatic activity when BCO1 was incubated with BC (20 μM) in the presence of emixustat (5 μM). In contrast, fenretinide, a known BCO1 inhibitor, efficiently inhibited the enzymatic activity of BCO1 (Fig. S5) (37). Thus, we concluded that RPE65 and BCO1 accommodate their respective substrates in different fashions and refrained from further predicting substrate binding.

Because of this limitation, we focused to the lipophilic mouth of the substrate tunnels. We reasoned that the diameter of the mouth of the BCO2 tunnel should be wider than that of BCO1 because BCO2 can accommodate bulky hydroxylated ionone ring sites. We identified Trp270 and Leu168 at the predicted tunnel entrance of BCO1 which were replaced by Phe and Gly in BCO2, respectively (Fig. 6a). These amino acids seem to diminish the diameter of the entrance of the substrate tunnel of BCO1. Sequence alignment confirmed that they were conserved among vertebrate family members (Fig. 6b). To test whether this difference contributed to substrate specificity, we performed site directed mutagenesis. We produced a BCO1 Trp270Phe mutant, and subsequently introduced a Leu168Gly mutation (Mut1 and Mut2m1). We then expressed the mutants and WT BCO1 in *E. coli* (Fig. 6c). Tests for enzymatic activity showed that both mutant variants converted BC to all-*trans*-retinal (Fig. 6d), demonstrating that the exchange did not impede BCO1's stability and/or catalytic activity.

To determine whether the exchange of these amino acids relaxed the substrate specificity of BCO1, we incubated the wild type and mutant BCO1 with ZEA, which is efficiently converted by BCO2 (Fig. S2d). Remarkably, mutant BCO1 variants readily converted zeaxanthin to all-*trans*-3-hydroxy-retinal in repeated assays whereas BCO1 did not show such enzymatic activity (Fig. 6e). Thus, we identified conserved amino acid residues in BCO1 and BCO2 which determine the specificity for different ionone rings of the substrates.

In conclusion, we provide evidence that the metabolism of the asymmetric provitamin A carotenoid CX is harmoniously achieved via two subsequent enzyme catalyzed chemical reactions. We show that this mechanism is made possible by ring site selectivity of the two CCDs: BCO1 interacts with the canonical β-ionone ring site and cleaves across the adjacent C15,C15' double bond. BCO2 preferentially interacts with 3-hydroxylated-ionone rings and cleaves across the adjacent C9',C10' double bond. We provide evidence that distinct amino acids in an overall conserved protein structure determine this ring site selectivity. In mouse intestine, we identified all metabolites of the proposed cleavage pathway upon CX supplementation. The described substrate specificity of BCO1 and BCO2 allow the metabolic conversion of many different carotenoids while ensuring the production of vitamin A. In future research, it remains to be elucidated whether the defined scheme for CX metabolism can be applied to the conversion of other asymmetric provitamins. With the large variety of carotenoids available in food, mammals require a reliable and robust mechanism for vitamin A production. This is essential for avoiding vitamin A deficiencies or hypercarotenoidemia and abberant effects of certain apocarotenoids.

METHODS

Animal care and husbandry.

Animal procedures and experiments were approved by the Case Western Reserve University Animal Care Committee. The generation of *Bco1*$^{-/-}$, *Bco2*$^{-/-}$, and *Isx*$^{-/-}$has been previously described (32, 33, 38). For the experiments, female *Bco1*$^{-/-}$(n=4), *Bco2*$^{-/-}$(n=4), and WT (n=3) mice (4–5 months of age) were fed a vitamin A deficient purified diet (AIN93G formulation, Research Diets Inc.) for two weeks. Then, mice were gavaged with CX (50 mg / kg body weight) in sesame oil 3 times over a 5 day period. An additional cohort of male *Isx*$^{-/-}$and WT mice (3 months of age) were starved overnight and gavaged one time with CX (n=3) or BC (n=3) (50 mg / kg body weight). Three hours after gavage, mice were anesthetized by intraperitoneal injection of a mixture containing ketamine 20 mg, Xylazine 7.5 mg, and sterile water or saline, with a dose of 0.2 ml per 25 g of mouse. Blood was drawn directly from the heart via cardiac puncture. Mice were then perfused with 20 mL PBS and killed by cervical dislocation. Blood and tissues were removed for analyses and/or snap frozen in liquid nitrogen and stored at -80˚C until use.

HPLC analysis of retinoids and carotenoids from animal samples.

Carotenoids and apocarotenoids were extracted from 100 μl of serum in 100 μl PBS or from 50 mg tissue homogenate in 200 μl PBS as previously described (26). In some analyses, lipids were saponified prior to extraction as described in (26). All HPLC analyses were performed on a normal-phase Zorbax Sil (5 μm, 4.6 × 150 mm) column. Chromatographic separation was achieved by isocratic flow (1.4 ml/min) of a mixture of ethyl acetate and hexane. For quantification of carotenoids and apocarotenoids, the HPLC column was scaled with known amounts of authentic standard substances. Mass spectrometry (MS)-based detection of 10,8'-diapocarotene-10,8'-dial was achieved with an LXQ linear ion trap mass spectrometer (Thermo Scientific, Waltham, MA) equipped with an atmospheric-pressure chemical ionization (APCI) interface coupled to an Agilent 1100 HPLC series (Agilent

Technologies) and diode array detector (Agilent Technologies). The HPLC effluent was directed into the MS via an APCI probe operated in the positive ionization mode.

q-RT-PCR analysis of BCO1 and BCO2 mRNA expression

Total RNA was isolated from jejunums from *Isx*$^{-/-}$ mice using TRIZOL reagent (Invitrogen, Carlsbad, CA). qPCR was carried out using an ABI Real Time PCR Instrument using BCO1 (Mm01251350) and BCO2 (Mm00460048) TaqMan probes (Applied BioSystems) as described in (24).

Expression of human BCO1 and murine BCO2 in E. coli.

Murine BCO2 or human BCO1 gene was cloned into a pTrcHis-TOPO expression vector (Invitrogen) using primer sets (BCO1: for, 5'-ATGGATATAATATTTGGCAGGAATAGG-3' and rev, 5'-GGTCAGAGGAGCCCCGTGGCA-3'; BCO2, for, 5'-ATGTTGGGACCGAAGCAAAGC-3' and rev, 5'-GATAGGCACAAAGGTGCCATG-3'). The plasmids were transformed into BL21 (DE3) competent *E. coli* (New England BioLabs) using a standard protocol. Transformed bacterial cells were grown in Luria Bertani broth at 37°C with constant shaking until reaching optical density of A_{600}=0.6. Protein production was induced in the cultured cells with the addition of 0.1 mM isopropyl-1-thio-β-d-galactopyranoside and 5 μM $FeSO_4$. The cells were allowed to grow overnight at 16°C (human BCO1) or for 8 hours at 16°C (murine BCO2).

Purification human BCO1 and murine BCO2.

Frozen cell pellets (-80°C) were thawed on ice and resuspended in buffer containing 50mM sodium phosphate, pH 7, 150 mM sodium chloride, 1 mM tris(2-carboxyethyl)phosphine hydrochloride (TCEP/HCl) (Hampton Research, Aliso Viejo, CA) and one cOmplete EDTA-free protease inhibitor mixture tablet (Roche Applied Science) at 4 ml/g. Cells were lysed by sonication (eight rounds of 1 min pulses with 1 min breaks at 30% maximum amplitude). The sonicated lysate was centrifuged at 21000 x g at 4°C for 30 min. The supernatant was loaded onto a 50 ml column containing 5 ml of Talon Co^{2+}-resin suspension (Takara Bio USA, Inc.) pre-equilibrated with 5 column volumes of ice cold buffer containing 50 mM sodium phosphate pH 7 with 300 mM NaCl, and 1 mM TCEP. Finally, bound proteins (BCO1 and BCO2) were eluted in ice-cold buffer containing 50 mM sodium phosphate, pH 7, with 300 mM NaCl and 1 mM TCEP, and 200 or 250 mM imidazole for BCO1 and BCO2, respectively. Eluted fractions were pooled and concentrated in a 50 kDA molecular weight cutoff Amicon® Ultra Centrifugal Filter (Millipore). The purified enzymes (0.125 mg x ml^{-1}) were stored at 4°C in buffer containing 50 mM sodium phosphate pH 7 with 150 mM NaCl, and 1 mM TCEP. The purity of the recombinant proteins was confirmed by 12% SDS-PAGE and by Western blotting using an AP conjugated anti-His antibody (Qiagen).

Enzyme assays with BCO1 and BCO2.

We performed enzyme assays under conditions where Michaelis Menten kinetics applies. These tests require specific initial rate conditions, i.e., very little product is formed and a substrate concentration far higher than the enzyme concentration. We also incubated the enzyme with the substrate for short time periods to guarantee time linearity of product

formation. APO10al, 3-hydroxy-APO10al, BC, AC, 15,15'-dehydro-BC, 20,20-di-nor-BC, and CX were a gift from DSM. Various concentrations of apocarotenoids and carotenoids dissolved in hexane were added to 33 μl ethanol containing 3% decyl maltose neopentyl glycol (DMN). The mixture was dried in a Vacufuge Plus (Eppendorf). 100 μL of purified enzyme (12 μg) solution (50 mM sodium phosphate pH 7 with 100 mM NaCl, and 1 mM TCEP) was added to the dried DMN carotenoid mixture, vortexed for 30 sec to form micelles, and incubated at 30°C for 12 min (BCO1) or 5 min (BCO2). The reactions were stopped by the addition of 100 μl water, 400 μl acetone, 400 μl diethyl ether, and 100 μl petroleum ether. After vortexing (30 sec), phase separation was achieved by centrifugation (3000 x g, 1 min, RT). The organic phase was collected and tried in a speedvac. The debris was dissolved in HPLC solvent and subjected to HPLC analysis. In some BCO1 enzyme assays, retinaldehydes were converted to the corresponding oximes. Briefly, 100 μl 2 M hydroxylamine (pH 8) and 200 μl methanol were added. After 10 min at RT, 400 μl acetone and 500 μl hexanes were added. After vortexing (30 sec), phase separation was achieved by centrifugation (3000 x g, 1 min, RT). The organic phase was dried and subjected to HPLC analysis. For inhibitor assays, BCO1 crude extract was incubated in the presence of 20 μM BC and 5 μM emixustat or 10 μM fenretinide in DMN micelles. Carotenoids and retinoids were then analyzed by HPLC as described above.

Kinetic analysis of BCO2.

150 μl of purified BCO2 enzyme (18 μg) solution was added to 50 μl enzyme assay buffer with 0.8% (v/v) Triton-X100. 3-hydroxy-APO8al or APO8al dissolved in 10 μl ethanol was added, and after brief vortexing (5 sec), incubated at 30ºC for 5 min. The reaction was stopped by the addition of 400 μl acetone (spiked with a 500 pmol BC internal standard), 400 μl diethyl ether, and 100 μl petroleum ether. Lipids were extracted as described above and subjected to HPLC analysis. Michaelis Menten kinetics were measured by performing this assay with concentrations of apocarotenoids ranging from 1.25 to 40 μM. Reaction velocity was calculated from the amount of product measured after 5 min, normalized based on the amount of BC measured as compared to a BC standard:

$$R = \frac{\Delta P \times \frac{BC_{STD}}{BC_S}}{\Delta t}$$

where R is the reaction rate, ΔP is the amount of product measured in pmol, BC_{STD} and BC_S are the areas under the BC curves at 460 nm in the standard and sample extract, respectively, and Δt is the duration of the reaction. MATLAB R2015b (MathWorks) and the Enzkin tool from the MathWorks File Exchange (MathWorks) were used to numerically calculate the parameters of the Michaelis Menten equation (K_m and V_{max}) from the data points for each run, and the averages of these parameters and confidence intervals were calculated and the Michaelis Menten curves were plotted (n=3). K_{cat} and K_{cat}/K_m were calculated from the numerically determined parameters and the final enzyme concentration.

Homology modeling.

FASTA sequences for human BCO1 and mouse BCO2 were acquired from the NCBI protein database, and homology models were created using SwissModel. The software chose the RPE65 dimer bound to 2 x Fe_2, 2 x emixustat and 2 x palmitate as the template for human BCO1, and the RPE62 dimer bound to 2 x Fe_2 in a lipid environment as the template for murine BCO2. In both cases, the BCO proteins modelled as dimers with sequence identities of 39.84% and 42.21% for BCO1 and BCO2, respectively. The PDB files were downloaded and molecular graphics and analyses were performed with the UCSF Chimera package. Chimera is developed by the Resource for Biocomputing, Visualization, and Informatics at the University of California, San Francisco (supported by NIGMS P41-GM103311). These structures were searched for structural differences at the substrate tunnel which may contribute to the substrate specificity of human BCO1.

Site directed mutagenesis.

The primers for mutagenesis were (for, 5'-CAGGCAGGAGGC**AA**AGCTCATTCTCC-3' and rev, 5'-GAGAATGAGCT**TT**GCCTCCTGCCTG-3') and (for, 5'-TGTGACGTTGCC**CC**ATTTACCGCCA-3', and rev, 5'-TGGCGGTAAAT**GG**GGCAACGTCACA-3') for the Trp270Phe and Leu168Gly mutations, respectively. Mutagenesis was performed using the QuikChange II XL Site-Directed Mutagenesis kit (Agilent) according to the manufacturer's instructions. Mutations were confirmed by Sanger sequencing and protein expression and enzyme assays with BC and ZEA were carried out as described above.

Supplementary Material

Refer to Web version on PubMed Central for supplementary material.

ACKNOWLEDGEMENTS

This work was supported by grants from National Eye Institute to J.v.L. (EY020551). The authors thank A. Wyss (DSM) for the gift of carotenoids and apo-carotenoids.

REFERENCES

1. Moise AR, Al-Babili S, and Wurtzel ET (2014) Mechanistic aspects of carotenoid biosynthesis, Chemical reviews 114, 164–193. [PubMed: 24175570]
2. Hou X, Rivers J, Leon P, McQuinn RP, and Pogson BJ (2016) Synthesis and Function of Apocarotenoid Signals in Plants, Trends Plant Sci 21, 792–803. [PubMed: 27344539]
3. Moise AR, von Lintig J, and Palczewski K (2005) Related enzymes solve evolutionarily recurrent problems in the metabolism of carotenoids, Trends Plant Sci 10, 178–186. [PubMed: 15817419]
4. Napoli JL (2012) Physiological insights into all-trans-retinoic acid biosynthesis, Biochim. Biophys. Acta 1821, 152–167. [PubMed: 21621639]
5. von Lintig J, and Wyss A (2001) Molecular analysis of vitamin A formation: cloning and characterization of beta-carotene 15,15'-dioxygenases, Arch. Biochem. Biophys 385, 47–52. [PubMed: 11361025]
6. Sui X, Kiser PD, Lintig J, and Palczewski K (2013) Structural basis of carotenoid cleavage: From bacteria to mammals, Arch. Biochem. Biophys 539, 203–213. [PubMed: 23827316]
7. Kloer DP, Ruch S, Al-Babili S, Beyer P, and Schulz GE (2005) The structure of a retinal-forming carotenoid oxygenase, Science 308, 267–269. [PubMed: 15821095]

8. Kiser PD, Golczak M, Lodowski DT, Chance MR, and Palczewski K (2009) Crystal structure of native RPE65, the retinoid isomerase of the visual cycle, Proc. Natl. Acad. Sci. U.S.A 106, 17325–17330. [PubMed: 19805034]

9. Borowski T, Blomberg MR, and Siegbahn PE (2008) Reaction mechanism of apocarotenoid oxygenase (ACO): a DFT study, Chemistry 14, 2264–2276. [PubMed: 18181127]

10. Kloer DP, and Schulz GE (2006) Structural and biological aspects of carotenoid cleavage, Cellular and molecular life sciences 63, 2291–2303. [PubMed: 16909205]

11. Sui X, Weitz AC, Farquhar ER, Badiee M, Banerjee S, von Lintig J, Tochtrop GP, Palczewski K, Hendrich MP, and Kiser PD (2017) Structure and Spectroscopy of Alkene-Cleaving Dioxygenases Containing an Atypically Coordinated Non-Heme Iron Center, Biochemistry 56, 2836–2852. [PubMed: 28493664]

12. Babino D, Golczak M, Kiser PD, Wyss A, Palczewski K, and von Lintig J (2016) The Biochemical Basis of Vitamin A3 Production in Arthropod Vision, ACS Chem. Biol 11, 1049–1057. [PubMed: 26811964]

13. Sui X, Golczak M, Zhang J, Kleinberg KA, von Lintig J, Palczewski K, and Kiser PD (2015) Utilization of Dioxygen by Carotenoid Cleavage Oxygenases, J. Biol. Chem 290, 30212–30223. [PubMed: 26499794]

14. Dela Sena C, Riedl KM, Narayanasamy S, Curley RW, Jr., Schwartz SJ, and Harrison EH (2014) The human enzyme that converts dietary provitamin a carotenoids to vitamin a is a dioxygenase, J. Biol. Chem 289, 13661–13666. [PubMed: 24668807]

15. von Lintig J (2010) Colors with functions: elucidating the biochemical and molecular basis of carotenoid metabolism, Annu. Rev. Nutr 30, 35–56. [PubMed: 20415581]

16. Kiefer C, Hessel S, Lampert JM, Vogt K, Lederer MO, Breithaupt DE, and von Lintig J (2001) Identification and characterization of a mammalian enzyme catalyzing the asymmetric oxidative cleavage of provitamin A, J. Biol. Chem 276, 14110–14116. [PubMed: 11278918]

17. Redmond TM, Poliakov E, Yu S, Tsai JY, Lu Z, and Gentleman S (2005) Mutation of key residues of RPE65 abolishes its enzymatic role as isomerohydrolase in the visual cycle, Proc. Natl. Acad. Sci. U.S.A 102, 13658–13663. [PubMed: 16150724]

18. Olson JA, and Krinsky NI (1995) Introduction: the colorful, fascinating world of the carotenoids: important physiologic modulators, FASEB. J 9, 1547–1550. [PubMed: 8529833]

19. Cooperstone JL, Goetz HJ, Riedl KM, Harrison EH, Schwartz SJ, and Kopec RE (2017) Relative contribution of alpha-carotene to postprandial vitamin A concentrations in healthy humans after carrot consumption, Am. J. Clin. Nutr 106, 59–66. [PubMed: 28515067]

20. Burri BJ, La Frano MR, and Zhu C (2016) Absorption, metabolism, and functions of beta-cryptoxanthin, Nutr. Rev 74, 69–82. [PubMed: 26747887]

21. Lindqvist A, and Andersson S (2002) Biochemical properties of purified recombinant human beta-carotene 15,15'-monooxygenase, J. Biol. Chem 277, 23942–23948. [PubMed: 11960992]

22. dela Sena C, Narayanasamy S, Riedl KM, Curley RW, Jr., Schwartz SJ, and Harrison EH (2013) Substrate specificity of purified recombinant human beta-carotene 15,15'-oxygenase (BCO1), J. Biol. Chem 288, 37094–37103. [PubMed: 24187135]

23. Hu KQ, Liu C, Ernst H, Krinsky NI, Russell RM, and Wang XD (2006) The biochemical characterization of ferret carotene-9',10'-monooxygenase catalyzing cleavage of carotenoids in vitro and in vivo, J. Biol. Chem 281, 19327–19338. [PubMed: 16672231]

24. Amengual J, Widjaja-Adhi MA, Rodriguez-Santiago S, Hessel S, Golczak M, Palczewski K, and von Lintig J (2013) Two carotenoid oxygenases contribute to mammalian provitamin A metabolism, J. Biol. Chem. 288, 34081–34096.

25. Dela Sena C, Sun J, Narayanasamy S, Riedl KM, Yuan Y, Curley RW, Jr., Schwartz SJ, and Harrison EH (2016) Substrate Specificity of Purified Recombinant Chicken beta-Carotene 9',10'-Oxygenase (BCO2), J. Biol. Chem 291, 14609–14619. [PubMed: 27143479]

26. Babino D, Palczewski G, Widjaja-Adhi MA, Kiser PD, Golczak M, and von Lintig J (2015) Characterization of the Role of beta-Carotene 9,10-Dioxygenase in Macular Pigment Metabolism, J. Biol. Chem 290, 24844–24857. [PubMed: 26307071]

27. Amengual J, Gouranton E, van Helden YG, Hessel S, Ribot J, Kramer E, Kiec-Wilk B, Razny U, Lietz G, Wyss A, Dembinska-Kiec A, Palou A, Keijer J, Landrier JF, Bonet ML, and von Lintig J

(2011) Beta-Carotene Reduces Body Adiposity of Mice via BCMO1, PloS one 6, e20644. [PubMed: 21673813]

28. Mein JR, Dolnikowski GG, Ernst H, Russell RM, and Wang XD (2010) Enzymatic formation of apo-carotenoids from the xanthophyll carotenoids lutein, zeaxanthin and beta-cryptoxanthin by ferret carotene-9',10'-monooxygenase, Arch. Biochem. Biophys 506, 109–121. [PubMed: 21081106]
29. Gartner W, Ullrich D, and Vogt K (1991) Quantum yield of CHAPSO-solubilized rhodopsin and 3-hydroxy retinal containing bovine opsin, Photochem. Photobiol 54, 1047–1055. [PubMed: 1837929]
30. Eroglu A, Hruszkewycz DP, Curley RW, Jr., and Harrison EH (2010) The eccentric cleavage product of beta-carotene, beta-apo-13-carotenone, functions as an antagonist of RXRalpha, Arch. Biochem. Biophys 504, 11–16. [PubMed: 20678466]
31. Eroglu A, Hruszkewycz DP, dela Sena C, Narayanasamy S, Riedl KM, Kopec RE, Schwartz SJ, Curley RW, Jr., and Harrison EH (2012) Naturally occurring eccentric cleavage products of provitamin A beta-carotene function as antagonists of retinoic acid receptors, J. Biol. Chem 287, 15886–15895. [PubMed: 22418437]
32. Hessel S, Eichinger A, Isken A, Amengual J, Hunzelmann S, Hoeller U, Elste V, Hunziker W, Goralczyk R, Oberhauser V, von Lintig J, and Wyss A (2007) CMO1 deficiency abolishes vitamin A production from beta-carotene and alters lipid metabolism in mice, J. Biol. Chem 282, 33553–33561. [PubMed: 17855355]
33. Amengual J, Lobo GP, Golczak M, Li HN, Klimova T, Hoppel CL, Wyss A, Palczewski K, and von Lintig J (2011) A mitochondrial enzyme degrades carotenoids and protects against oxidative stress, FASEB J 25, 948–959. [PubMed: 21106934]
34. Ford NA, Clinton SK, von Lintig J, Wyss A, and Erdman JW, Jr. (2010) Loss of carotene-9',10'-monooxygenase expression increases serum and tissue lycopene concentrations in lycopene-fed mice, J. Nutr 140, 2134–2138. [PubMed: 20962153]
35. Widjaja-Adhi MAK, Palczewski G, Dale K, Knauss EA, Kelly ME, Golczak M, Levine AD, and von Lintig J (2017) Transcription factor ISX mediates the cross talk between diet and immunity, Proc. Natl. Acad. Sci. U. S. A 114, 11530–11535. [PubMed: 29073082]
36. Kiser PD, Zhang J, Badiee M, Li Q, Shi W, Sui X, Golczak M, Tochtrop GP, and Palczewski K (2015) Catalytic mechanism of a retinoid isomerase essential for vertebrate vision, Nature chemical biology 11, 409–415. [PubMed: 25894083]
37. Lobo GP, Amengual J, Li HN, Golczak M, Bonet ML, Palczewski K, and von Lintig J (2010) {beta},{beta}-Carotene Decreases Peroxisome Proliferator Receptor {gamma} Activity and Reduces Lipid Storage Capacity of Adipocytes in a {beta},{beta}-Carotene Oxygenase 1-dependent Manner, J. Biol. Chem 285, 27891–27899. [PubMed: 20573961]
38. Choi MY, Romer AI, Hu M, Lepourcelet M, Mechoor A, Yesilaltay A, Krieger M, Gray PA, and Shivdasani RA (2006) A dynamic expression survey identifies transcription factors relevant in mouse digestive tract development, Development 133, 4119–4129. [PubMed: 16971476]

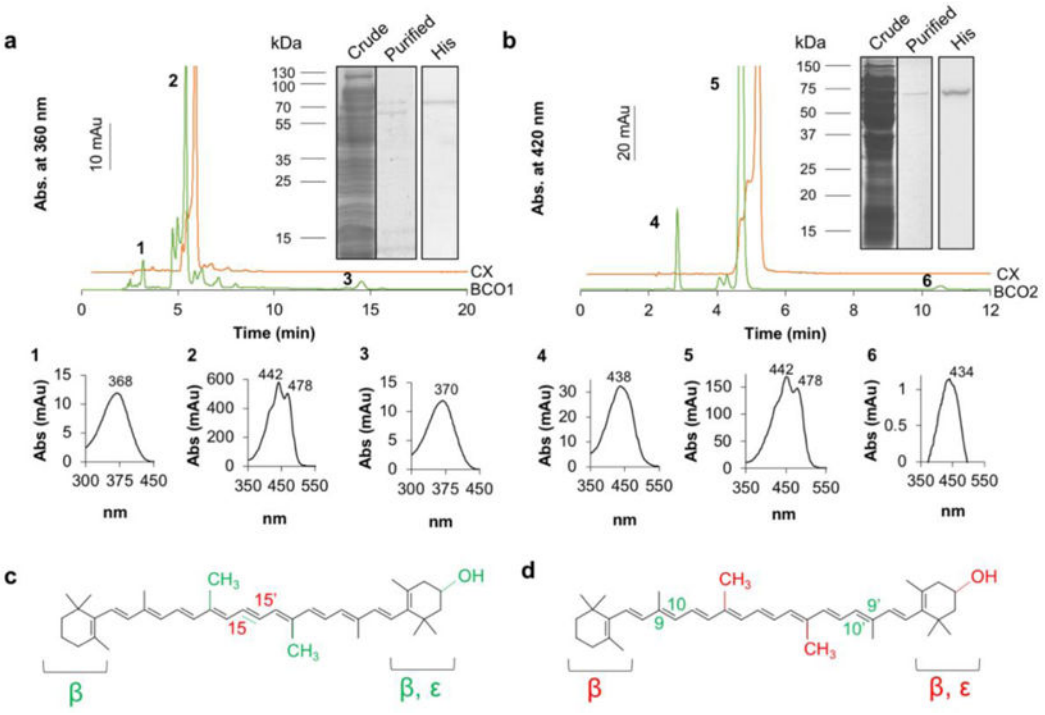

Figure 1. Oxidative conversion of provitamin A carotenoids by BCO1 and BCO2.

a. Recombinant human BCO1 was purified by affinity chromatography as shown by Coomassie stained SDS-PAGE (crude extract and purified fraction). The identity of the enzyme was confirmed by Western blot analysis with anti-His-tag antibodies (His). HPLC trace at 360 nm of a lipid extract of the incubation of BCO1 and CX (green) and CX alone (orange) showed that BCO1 converted CX (peak 2) into RAL (peak 1) and 3-OH-RAL (peak 3). Below the traces are the corresponding spectra of peaks 1 to 3. **b.** Recombinant BCO2 was purified by affinity chromatography as shown by Coomassie stained SDS-PAGE (crude extract and purified fractions). The identity of the enzyme was confirmed by Western blot analysis with anti-His-tag antibodies (His). HPLC trace at 420 nm of a lipid extract of the incubation of BCO2 and CX (green) and CX alone (orange) showed that BCO2 converted CX (peak 5) into APO10al (peak 4) and 3-hydroxy-APO10al (peak 6). Below the HPLC traces are the corresponding spectra of peaks 4 to 6. **c.** Scheme of substrates used to analyze the activity of recombinant human BCO1. The displayed structure highlights in green the tested chemical modifications of BCO1's classical substrate BC. These modifications include 3-hydroxy substitutions of the β-ionone ring, replacement of the β-by an ε-ionone, removal of methyl groups (nor), or replacement of the scissile bond with a triple bond. The central cleavage site at position C15,C15' of BCO1 is indicated in red. Respective enzyme assays are presented in supplemental figure 2. **d.** Scheme of substrates used to analyze the activity of recombinant human BCO2. The structure highlights in red the tested chemical modifications of BCO2's classical substrate BC. These modifications include 3-hydroxy substitutions of the β-ionone ring, replacement of the β-by an ε-ionone, or removal of methyl groups (nor). The eccentric cleavage sites at positions C9,C10 and C9',C10' of BCO2 are indicated in green. Respective enzyme assays are presented in supplemental figure 1.

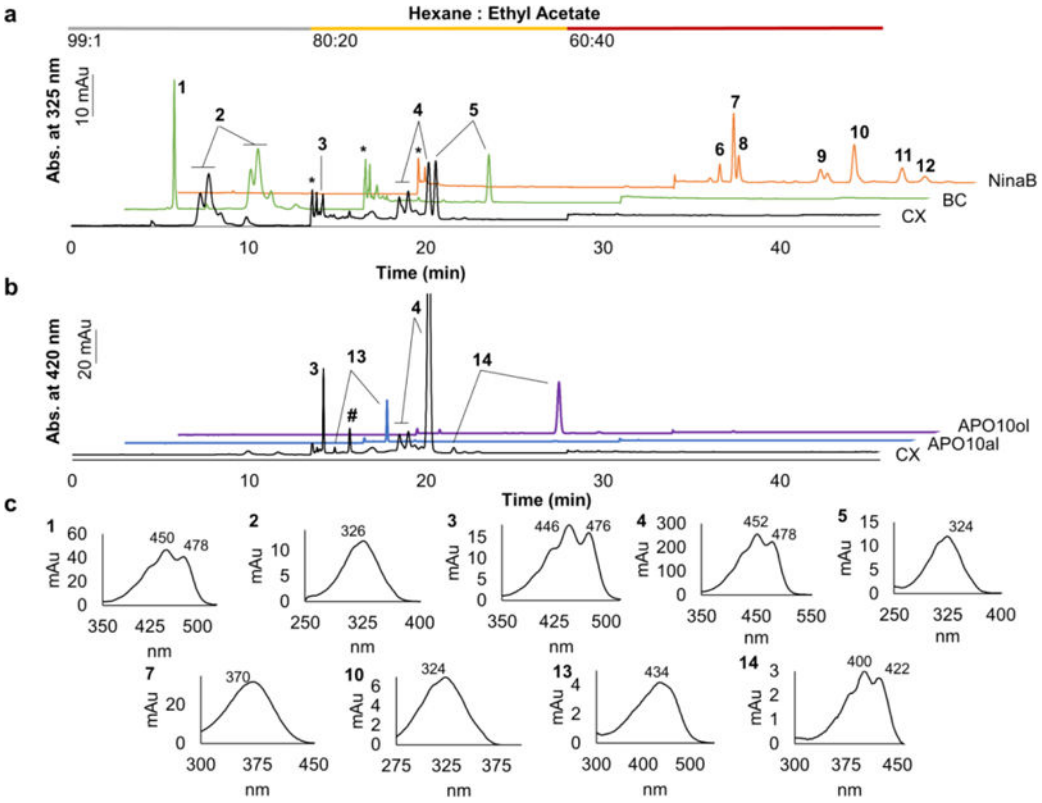

Figure 2. Provitamin A carotenoid metabolism in the intestine of of *Isx*$^{-/-}$ mice.

Shown are HPLC traces of intestinal lipid extracts from mice. **a.** A three step gradient HPLC system was applied to separate nonpolar (0 to 12 min), slightly polar (12 to 28 min) and polar (28 to 44 min) carotenoids and apocarotenoids by mixing hexane with ethyl acetate at different ratios (indicated at the top of the diagram). The diagram displays the HPLC trace at 325 nm of lipid extracts of *Isx*$^{-/-}$ mice supplemented with CX (black trace) or BC (green trace). The orange trace represents a lipid extract of an enzyme assay of insect NinaB incubated with ZEA. Peaks were identified by retention time and spectral characteristics. **b.** The diagram displays the HPLC trace at 420 nm of a lipid extract of *Isx*$^{-/-}$ mice supplemented with CX (black trace). The blue trace represents the APO10al and the purple trace the APO10ol standard. **c.** Spectral characteristics of peaks identified in **a** and **b** are shown. The individual peaks represent 1, BC; 2, retinyl ester; 3, 3-oxo-CX; 4, CX (includes both all-*trans* and *cis* isomers); 5, all-*trans*-retinol; 6, 3-hydroxy-13-*cis*-retinal; 7, all-*trans*-3-hydroxy-retinal; 8, 11-*cis*-3-hydroxy-retinal; 9, ZEA; 10, all-3-hydroxy-*trans*-retinol; 11, 11-*cis*-3-hydroxy-retinol; 12, ZEA isomer; 13, APO10al; 14, APO10ol; *, solvent peak; #, unidentified peak.

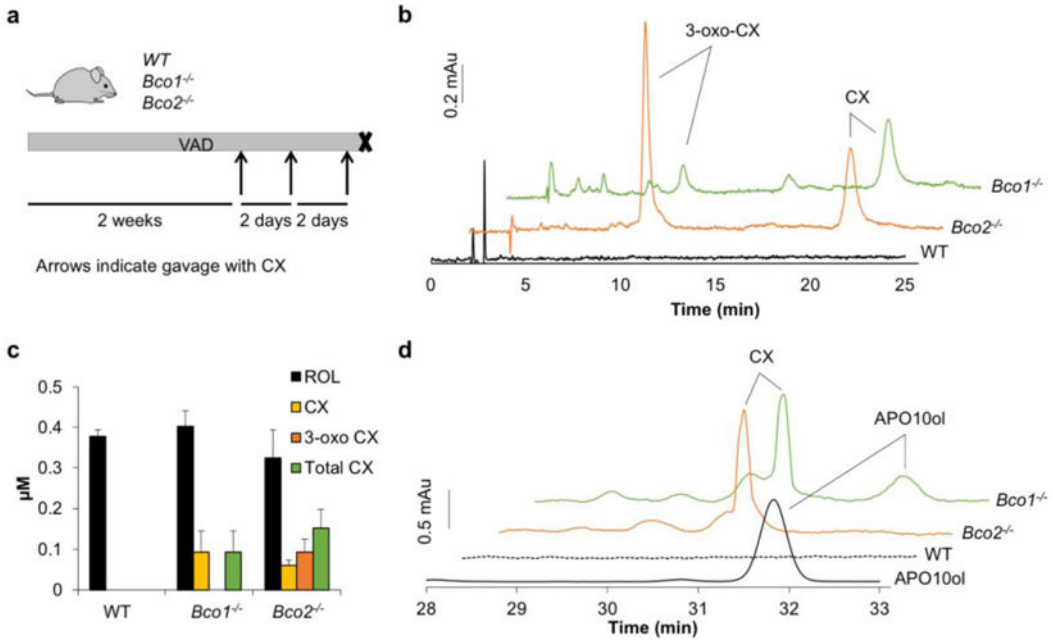

Figure 3. Analyses of CX metabolism in *Bco1* and *Bco2* knockout mice.

a. WT, *Bco1*$^{-/-}$, and *Bco2*$^{-/-}$mice were maintained on a vitamin A deficient diet for 2 weeks, and then while still on the vitamin A deficient diet were gavaged with CX (50 mg/kg body weight) in sesame oil every two days for a total of three doses. At the end of this period, mice were sacrificed, and their sera and livers were collected. **b.** Representative HPLC traces at 420 nn of lipid extracts from serum of wild type (WT) (black), *Bco2*$^{-/-}$(orange), and *Bco1*$^{-/-}$(green) mice. CX accumulated in both mutant strains, 3-oxo-CX accumulated in *Bco2*$^{-/-}$mice, and no carotenoids were detected in WT mice supplemented with CX. **c.** Quantification CX (yellow), 3-oxo CX (orange), total CX (green), and all-trans-retinol (ROL) (black) in serum of WT, *Bco1*$^{-/-}$, and *Bco2*$^{-/-}$mice. The graph represents mean values from *Bco1*$^{-/-}$(n=4), *Bco2*$^{-/-}$(n=4), and WT (n=3) mice +/-SD. **d.** HPLC traces at 420 nm of hepatic lipid extracts of WT (black dashed), *Bco2*$^{-/-}$(orange) or *Bco1*$^{-/-}$(green) mice. An HPLC trace of an APO10ol standard is shown in solid black. Note that CX accumulated in both mutant strains, but APO10ol only was detectable in *Bco2*$^{-/-}$mice. No carotenoids or apocarotenoids were detected in WT mice supplemented with CX.

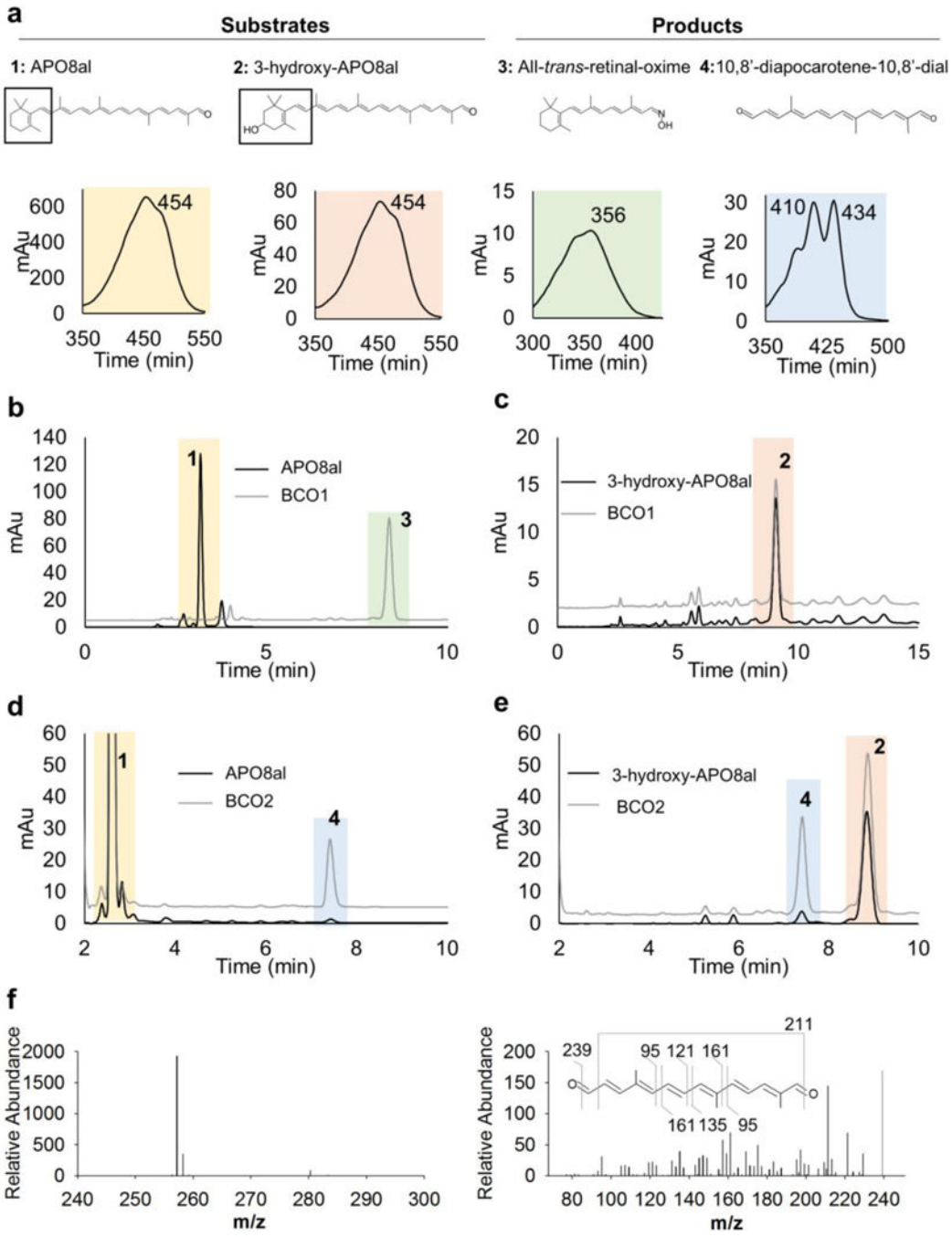

Figure 4. Ionone ring site selectivity of recombinant BCO1 and BCO2.

a. Chemical structures and spectral characteristics of substrates (1, β-apo-8'-carotenal, APO10al; 2, 3-hydroxy-β-apo-8'-carotenal, 3-hydroxy-APO10al) and products (3, All-*trans*-retinal-oxime; 4, 10,8'-diapocarotene-10,8'-dial) of enzymatic assays with BCO1 and BCO2 as described in B-E. **b-c**. HPLC traces at 360 nm of lipid extracts of enzyme assays with human BCO1 and APO10al (**b**) and 3-hydroxy-APO10al (**C**) (black traces). The substrates without enzyme incubation are shown as grey traces. Incubation of BCO1 with APO8al (1) produced all-*trans*-retinal-oxime (3). Incubation of BCO1 with 3-hydroxy-APO8al (2)

produced no cleavage products. **d-e.** HPLC traces at 420 nm of lipid extracts of enzyme assays with murine BCO2 and APO10al (**d**) and 3-hydroxy-APO10al (**e**) (black traces). The substrates without enzyme incubation are shown grey traces. Incubation of BCO2 with APO8al (1) produced 10,8'-diapocarotene-10,8'-dial (4). Incubation of BCO2 with 3-hydroxy-APO8al (2) produced 10,8'-diapocarotene-10,8'-dial l (4). MS/MS analysis in MS^+ mode verified the identity of the 10,8'-diapocarotene-10,8'-dial resulting from the incubation of BCO2 with either apocarotenoid. The compound displayed a molecular mass of 257 Daltons and a characteristic MS/MS fragmentation pattern.

a

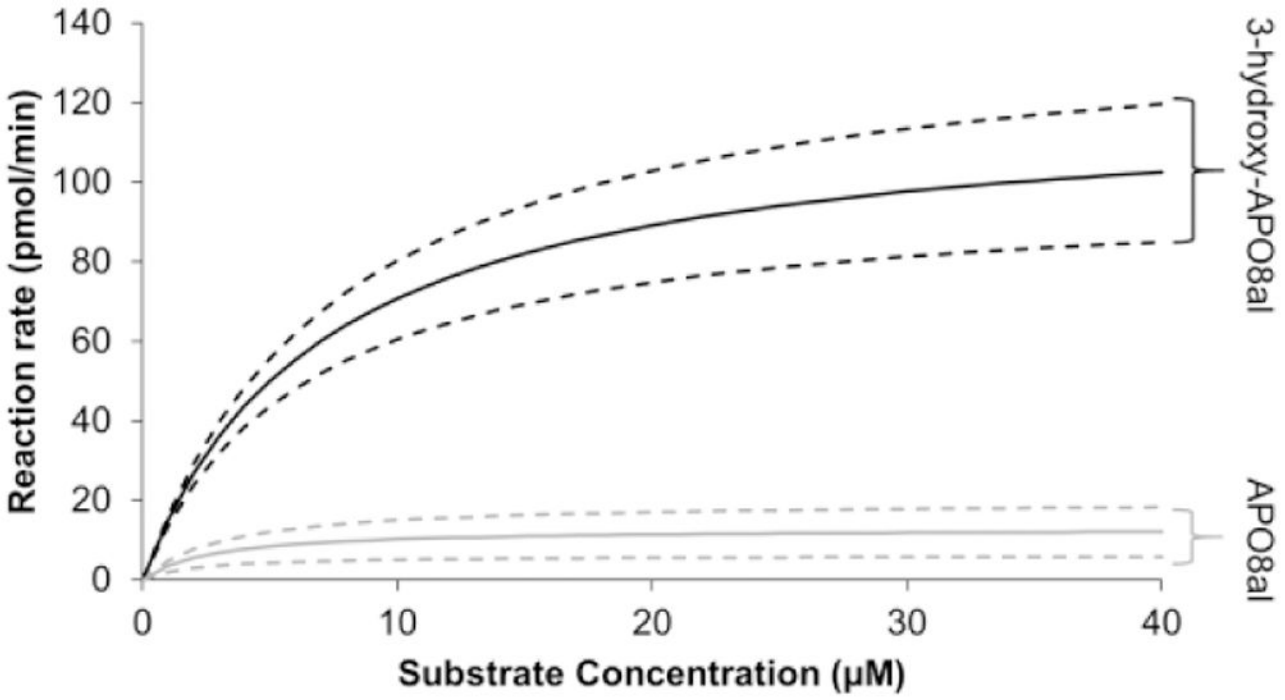

b

	3-hydroxy-APO8al				APO8al			
	K_m (μM)	K_{cat} (s^{-1})	V_{max} (pmol/s)	K_{cat}/K_m ($s^{-1}M^{-1}$)	K_m (μM)	K_{cat} (s^{-1})	V_{max} (pmol/s)	K_{cat}/K_m ($s^{-1}M^{-1}$)
Average	7.03	0.83	2.01	$1.18x10^5$	2.61	.091	0.21	$3.49x10^4$
St. Dev.	0.40	.098	0.23	$1.47x10^4$	0.27	.026	0.06	$1.06x10^4$

Figure 5. Kinetic analysis of recombinant BCO2 with apocarotenoid substrates.

a. Michaelis Menten kinetic analyses of recombinant purified murine BCO2 incubated with increasing amounts (1.25–40 μM) of 3-hydroxy-APO8al (black) and APO8al (grey). Solid lines depict the Michaelis Menten curve with average parameters numerically calculated using MATLAB, and the dashed lines depict the 95% confidence interval. **b.** The table shows average +/-standard deviation values of K_m, K_{cat}, V_{max}, and K_{cat}/K_m calculated from three independent kinetic analyses.

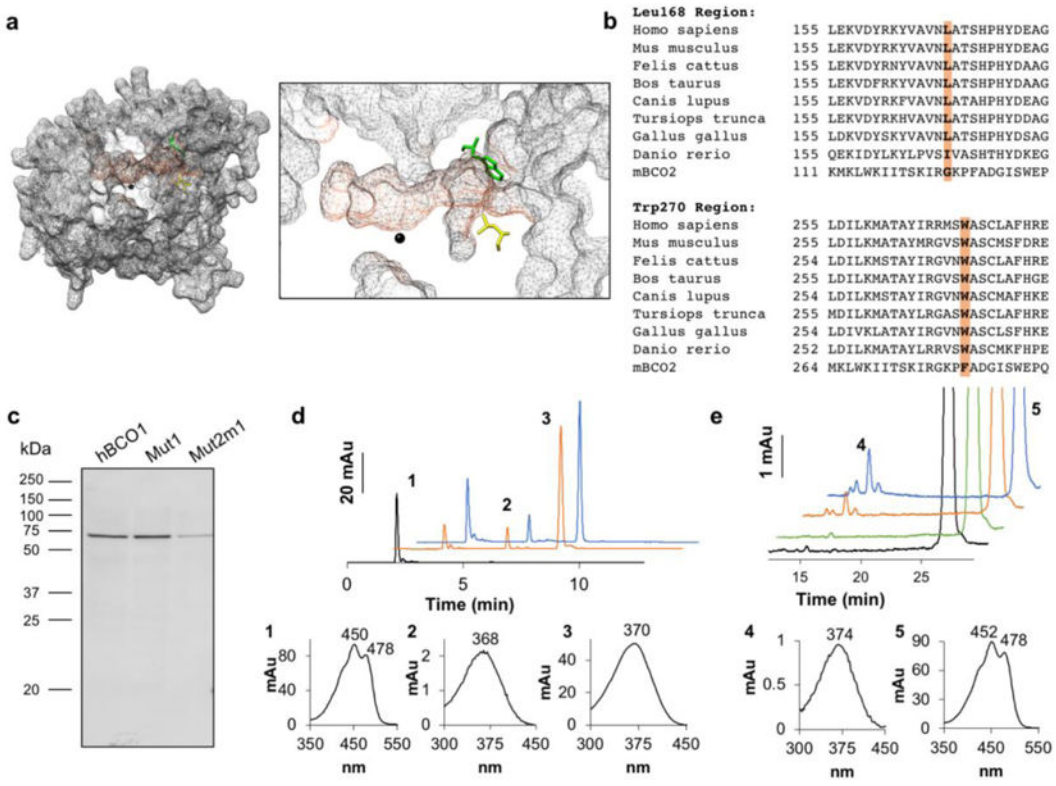

Figure 6. Homology modeling, sequence analysis, and mutagenesis of BCO1 indicate amino acid residues which contribute to the substrate specificity of BCO1.

a. Surface mesh rendering of the homology model of human BCO1 (grey). The predicted substrate tunnel is highlighted (orange). At the entrance to the predicted substrate tunnel, leucine (Leu) 168 (yellow) and tryptophan (Trp) 270 (green) are shown, and the iron cofactor in the active site is indicated in black. A magnified visualization of the predicated substrate tunnel is shown on the right. b. BCO1 and BCO2 sequence alignments of different vertebrates showed that Leu168 and Trp270 are well conserved across species (orange). In BCO2 these amino acids are replaced by glycine (Gly) and phenylalanine (Phe), respectively. c. The human BCO1 mutant Trp270Phe (Mut1) and double mutant Trp270Phe + Leu168Gly (Mut2m1) as well as the original human BCO1 construct were expressed in *E. coli* and the expression of the proteins were confirmed by Western blotting of the crude protein extract (20 μg per lane) with an anti-His antibody. d. Mut1 and Mut2m1 protein extracts were incubated with BC. The diagram shows HPLC traces at 360 nm of BC without incubation (black), and upon incubation with Mut1 (orange) and Mut2m1 (blue). Peak 1, BC; peak 2, 13-*cis*-retinal; and peak 3, all-*trans*-retinal. The spectral characteristics of peaks 1 to 3 are shown underneath the diagram with the HPLC traces. e. Wild type (WT), Mut1, and Mut2m1 protein extracts were incubated with ZEA. The diagram shows HPLC traces at 360 nm of ZEA without incubation (black), and upon incubation with WT (green), Mut1 (orange) and Mut2m1 (blue). Peak 4, all-*trans*-3-hydroxy-retinal and peak 5, ZEA. The spectral characteristics of peaks 4 and 5 are shown underneath the diagram with the HPLC traces.